2020

Neuromodulation of Spinal Pathways Involved in Chronic Pain: Implications for Motor Rehabilitation

Taylor Ray Mayberry
Medical University of South Carolina

Neuromodulation of Spinal Pathways Involved in Chronic Pain: Implications for Motor Rehabilitation

Taylor Ray Mayberry

A thesis submitted to the faculty of the Medical University of South Carolina in partial fulfillment of the requirements for the degree of Master of Science in Biomedical Science in the College of Graduate Studies.

Department of Neuroscience

2020

Approved by:

Chairman, Advisory Committee

_____

Nathan C. Rowland

_____

Mark G. Bowden

_____

Aiko K. Thompson

_____

Brett E. Froeliger

TABLE OF CONTENTS

List of Figures

LIST OF TABLES

Taylor Ray Mayberry. Neuromodulation of Spinal Pathways Involved in Chronic Pain: Implications for Motor Rehabilitation. (Under the direction of Nathan C. Rowland).

Lower thoracic dorsal column epidural stimulation is a common intervention in the treatment of chronic low back and leg pain (CLBLP). This has traditionally been carried out using low frequency (1-100 Hz) tonic stimulation (LFTS). LFTS has also been studied in the context of spinal cord injury (SCI) and has been found to selectively activate motor nerve roots in persons with paraplegia, some of whom have regained partial ambulation using this technique. A known adverse effect of LFTS is attenuation of proprioception. Recent advancements in spinal cord stimulation (SCS) technology using high frequency (1-10 kHz) burst stimulation (HFBS) have demonstrated pain mitigation comparable to LFTS, however effects on motor neuron and proprioceptive activity using this new modality are poorly understood. For this thesis work, one individual with CLBLP underwent electromyography (EMG) recording from lower extremity muscles during intraoperative SCS placement (Spectra WaveWriter™, Boston Scientific, Marlborough, MA) to investigate pain mitigation and motor neuron activation in response to HFBS. Proprioception was also tested extraoperatively using a threshold to detect passive motion (TTDPM) protocol in which LFTS and HFBS were compared with respect to perception of movement around the knee joint. Finally, the subject performed a gait task on an instrumented treadmill while recording EMG from lower extremity muscles and switching between SCS modalities. Extraoperative SCS testing at rest revealed that HFBS correlated with a significant increase in EMG amplitude ($p < 0.01$) and decreased interpeak interval (IPI) ($p < 0.01$) of evoked potentials compared to LFTS. TTDPM showed similarity between HFBS and no stimulation, while LFTS resulted in reduced capacity to perceive change in passive knee flexion/extension ($p < 0.01$). EMG analysis showed thoracic SCS with HFBS, but not LFTS, did not alter normal gait patterns, including foot swing and step height ($p < 0.01$). Our results indicate that thoracic HFBS

may influence motor neuron activity without attenuating important proprioception signaling compared to LFTS and may represent a potential therapeutic modality for simultaneous treatment of chronic pain and motor recovery using SCS.

1.0 INTRODUCTION

Chronic low back and leg pain (CLBLP) is a leading cause of disability worldwide, and an estimated 34,000 spinal cord stimulation (SCS) surgeries are performed annually to alleviate debilitating CLBLP.[1] Approved by the FDA in 1989 for the treatment of chronic neuropathic pain, SCS modulates excitability of large, low-threshold Aβ fibers (non-nociceptive) along the dorsal column which synapse onto interneurons that inhibit ascending pain transmission toward the brain. Although traditional mechanistic explanations of SCS for treatment of CLBLP, such as the gate control theory, are widely accepted, stimulator technology that has emerged in the last decade is far less understood. For example, pain reduction via SCS has traditionally utilized low-frequency tonic stimulation (LFTS), which is generally applied at frequencies less than 100 Hz and produces paresthesias (i.e., a tingling sensation) at sensory threshold amplitudes thought to be necessary for targeting areas of pain.[2] However, recent evidence suggests that the induction of paresthesias via LFTS may compromise proprioceptive information flowing from the periphery to the spinal cord, thus potentially adversely modulating spinal projections involved in motor behaviors such as standing and walking.[3,4] In contrast, recent studies suggest higher frequencies (e.g., up to 10,000 Hz) and complex waveforms of stimulation such as high-frequency burst stimulation (HFBS) can attenuate pain perception without producing paresthesias. Nevertheless, the potential effect of HFBS on proprioceptive signaling and ability to influence ventral motoneuron (MN) pools has only recently begun to be investigated.

Motoneurons residing in the ventral aspect of the spinal cord rely on descending drive from the brain and afferent input from the periphery to shape voluntary movement.[5] In 2009, Harkema et al investigated the effects of SCS on MN activation utilizing LFTS ranging from 5-60 Hz (frequency) in subjects with complete spinal cord injury (SCI). LFTS of the lumbosacral spinal cord segments (T11 - L2) was found to elicit activation in

lower extremity musculature previously thought to be quiescent in these spinal cord injured individuals. In one subject, surface electromyography (EMG) showed that SCS facilitated activation of extensors during assisted standing, rhythmic activity during assisted walking and appropriate modulation of on/off states during assisted weight shifting tasks.[6] Notwithstanding, Formento et al found that LFTS interrupts proprioceptive sensory information from the lower extremities that helps shape motor activity. The amount of compromised afferent information during traditional spinal cord stimulation via LFTS was postulated to be dependent on the quantity of dorsal column primary afferents recruited and proportional to increases in current and pulse width.[3] In the Formento study, 3 subjects were implanted with a 16-contact epidural paddle array and implantable pulse generator (IPG) (Activa RC, Medtronic, Fridley, Minnesota) along the lumbosacral spinal cord (T11 – L2). Proprioception was tested using an isokinetic dynamometer to passively flex and extend the knee while subjects were seated. Knee flexion/extension was applied until subjects reported perceiving movement. Compared to no stimulation, LFTS parameters (15-100 Hz, 210–450 μs, 4.5–9.0 mA) were found to cause a significant loss ($p < .05$) of perceived position sense during passive movement when stimulation amplitudes were high enough to innervate their homonymous motor neuron pool to activation threshold (as measured by EMG). Interestingly, in the same study, although the epidural stimulator used during proprioceptive testing was only capable of stimulating at 125 Hz, by interleaving 4 stimulation programs with a 2 ms delay the group was able to create a 4-pulse 500 Hz bursting pattern. HFBS at 500Hz was found to elicit motor neuron activation with a 39.8% reduction in current amplitude when compared to 20 Hz LFTS. These two studies together demonstrate that while SCS is designed to directly modulate dorsal column pathways, a better understanding of exactly how fibers and neuronal pools are stimulated might possibly allow activation of

both ventral and dorsal columns in a way that benefits motor and sensory information processing.

Since the epidural space is exposed during surgical placement of the SCS device, information about a subject's motor and sensory spinal pathways can be easily obtained during the regular course of the procedure and compared to proprioceptive and motor responses once the subject is awake and moving with the device turned on. Our lab specializes in electrophysiological recordings in subjects undergoing spinal cord stimulator (SCS) implantation for CLBLP, while the Locomotion Laboratory at the Medical University of South Carolina (MUSC) specializes in quantifying proprioception and movement in human subjects. In order to examine potential differences in modulating sensorimotor pathways between traditional LFTS and newly developed HFBS parameters, this project investigated 3 specific aims:

Aim 1. Investigate the effect of LFTS on sensory thresholds intraoperatively. **Question: Does LFTS modulate the activity of ascending sensorimotor pathways?** In this aim, we measured somatosensory evoked potential thresholds in a subject undergoing SCS implantation during stimulation of epidural paddle contacts. *We hypothesized that LFTS would reduce somatosensory evoked potential thresholds.*

Aim 2. Determine the effect of HFBS on proprioceptive afferent signaling from the lower extremities. **Question: Does HFBS, when compared to traditional LFTS, allow for increased spatial limb awareness during passive motion?** In this aim, the postoperative subject from SA1 underwent isokinetic passive proprioceptive testing before and during spinal cord stimulation with HFBS and LFTS parameters targeting sensation surrounding the knee. *We hypothesized that the subject would have increased awareness of the lower limb in space through passive movement during optimal HFBS compared to optimal LFTS parameters.*

Aim 3. Determine the effect of HFBS on lower extremity muscle activity during gait. **Question: Does HFBS, when compared to LFTS, differentially affect muscle synergy patterns during gait?** In this aim, the subject from SA1 and SA2 performed treadmill walking before and during SCS stimulation. The subject was monitored with surface EMG and 3-D kinematic tracking software to quantify changes in gait pattern. *We hypothesized that the subject would have increased EMG module complexity during gait with HFBS compared to LFTS or no stimulation.*

If we are able to identify HFBS parameters that preserve proprioceptive signaling while attenuating pain, in future studies we may be able to apply these parameters for simultaneous treatment of neuropathic pain and movement rehabilitation in patients with chronic motor dysfunction, such as those with spinal cord injury and stroke.

1.1 Pain Signaling

Pain signaling involves nociceptor-triggered action potentials along Aδ and C primary afferent fibers in response to physical and chemical insult (Fig.1). As a result of activation of nociceptive fibers, glutamate and substance P are released within lamina I and II of the dorsal horn of the spinal cord (DHSC)(Fig. 2). [9,10]

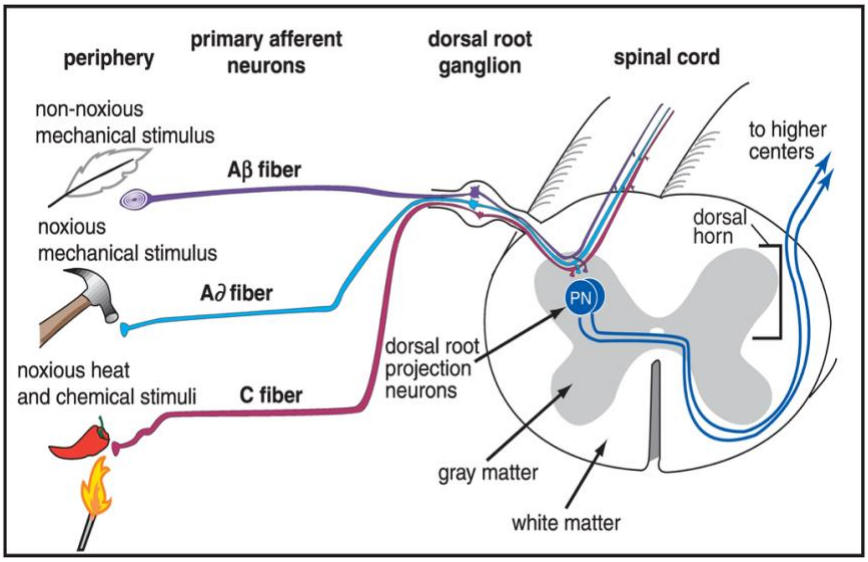

Figure 1: Image and caption modified from [7]. Illustration of nociceptive signaling to the dorsal horn of the spinal cord.

Within the DHSC, 2nd order fibers carrying pain signals cross the midline and ascend as part of the anterolateral system (i.e., spinothalamic, spinoreticular and spinomesencephalic tracts) where axons synapse within the midbrain and thalamus for pain perception processing.[11]

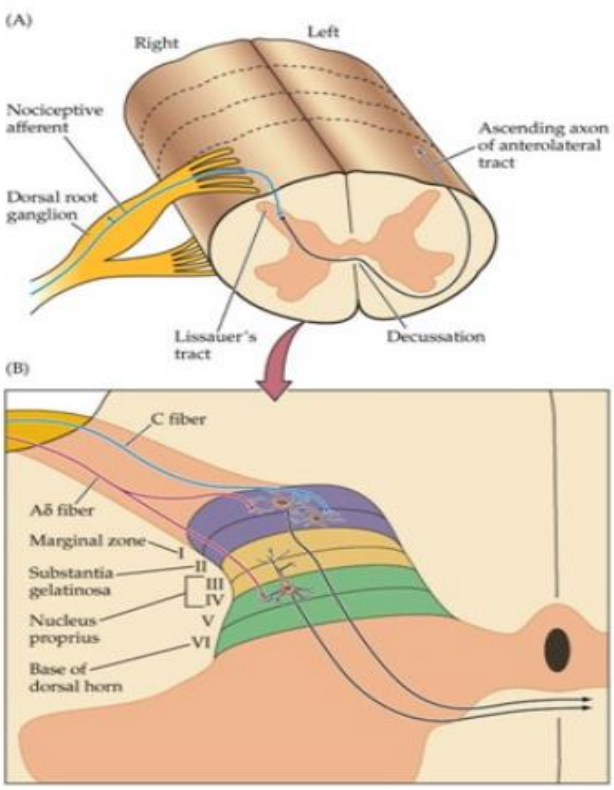

Figure 2: Image and caption modified from [8]. Illustration of lamina I-VI of the DHSC, with nociceptive C-fibers terminating in lamina I-II.

1.1.1 Chronic Pain

Chronic pain is defined by the International Association for the Study of Pain (IASP) and World Health Organization (WHO) as pain that persists beyond the normal time of healing and is clinically recognized by debilitating pain longer than three months in more than one anatomical location (e.g., low back and leg).[12] Chronic pain was identified as one of the top causes of disability in the world in the 2017 Global Burden of Disease Study compiled by the Institute for Health Metrics and Evaluation.[13] Chronic pain may be further delineated into a subcategory of pain relating specifically to damage of the peripheral or central nervous system. The current International Classification of Diseases (ICD-11) defines chronic neuropathic pain as pain caused by a lesion or disease of the somatosensory nervous system.[14] Chronic neuropathic pain is generally thought to be caused by dysregulation of nociceptive signaling and can lead to normal mechanical stimuli being perceived as painful (allodynia) or painful stimuli being perceived as a much higher intensity of pain

(hyperalgesia). Plasticity in the neuron, interneuron, microglia and astrocyte complexes within the DHSC stemming from repeated exposure to glutamate and substance P release is thought to play critical roles in this dysregulation.[15] Existing homeostatic mechanisms used to regulate pain perception may be altered in persons suffering from chronic pain. Inhibitory interneurons within the superficial laminae of the DHSC have GABAergic projections to 2nd order neurons responsible for modulating pain transmission to higher brain centers. These inhibitory interneurons are thought to be regulated by primary nociceptive (Aδ and C) and mechanoreceptor (Aβ) afferent fibers, with loss of this tight regulation leading to excessive pain perception. Another potential mechanism of chronic pain suggests involvement of the inflammatory cascade. In rodents, Substance P injection showed significant decrease in pain response time ($p < .05$) to painful stimulus applied to the hind paw compared to saline injection.[16] In humans, Hagermark et al showed a localized inflammatory response to intradermal injection of substance P.[17] Using transgenic mice that allowed for ablation of microglia expressing CX_3CR1^+ (chemokine receptor), Peng and colleagues investigated the role of microglia within the DHSC following spinal nerve transection (SNT). Immediately following SNT, hind paw withdrawal reflex to noxious thermal stimuli showed no significant difference among control and microglia ablated mice. However, three days post-SNT, control mice showed significant decrease in withdrawal latency to noxious stimuli ($p < .001$) compared to the knockout group.[18] Together, these studies indicate that inflammatory response from acute peripheral nerve injury may facilitate cellular changes that increase excitability of nociceptive pathways and highlight the complex chain of events involved in the transition of acute to chronic pain.

1.1.2 GATE CONTROL THEORY

Important work published in 1965 by Melzack et al on the relationship between mechanosensory afferents and pain within the DHSC continues to serve as the best accepted model for the regulation of pain signaling nearly a half-century later. Known as the Gate Control Theory (GCT), Melzack postulated that Aβ fibers inhibit 2nd order pain-signaling neurons resulting in reduced transmission of these signals to higher order centers. (Fig.3).[19] According to Melzack's theory, this reduction involves inhibitory interneurons within the DHSC. Clinicians tested Melzack's theory by directly modulating Aβ fiber axons along the dorsal column pathway using electrical current, eventually leading to the development of spinal cord stimulation (SCS) as an effective intervention for CLBLP.[20]

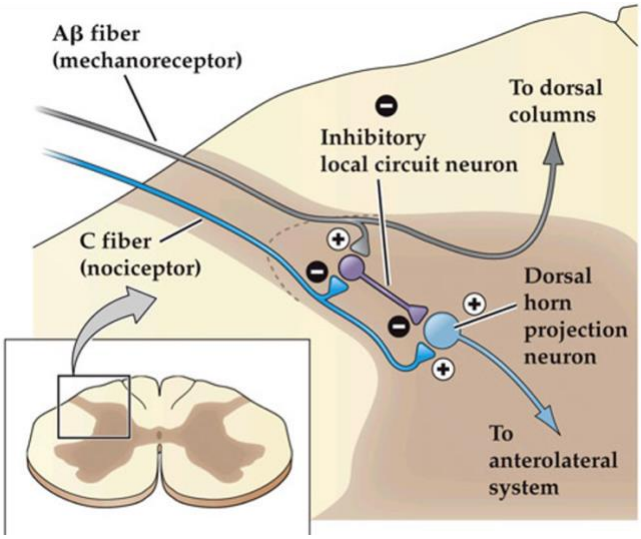

Figure 3: Image and caption modified from [8]. Model showing a simplified mechanism of pain projection inhibition through Aβ fiber activation of dorsal horn inhibitory interneurons

1.2 SPINAL CORD STIMULATION PARAMETERS FOR CHRONIC PAIN

SCS is currently used to treat chronic neuropathic pain that may arise from spinal injury, disease, and/or previous spinal surgery, for example, in cases of post-laminectomy syndrome, the most common indication for SCS. SCS surgery represents 70% of all neuromodulation cases in the United States and is expected to grow as the intervention shows continued promise to successfully treat neuropathic pain from these and many other etiologies.[1] The SCS procedure for CLBLP involves lower thoracic placement of epidural electrodes via laminectomy that, when activated, excite Aβ fibers, producing a paresthetic sensation along the region of pain. Traditional application of

SCS utilized a pattern of electrical impulses known as tonic (constant) stimulation, which is comprised of three main parameters that in combination determine the intensity of the stimulus: frequency (Hz), pulse width (μs) and amplitude (mA) (Fig.4).

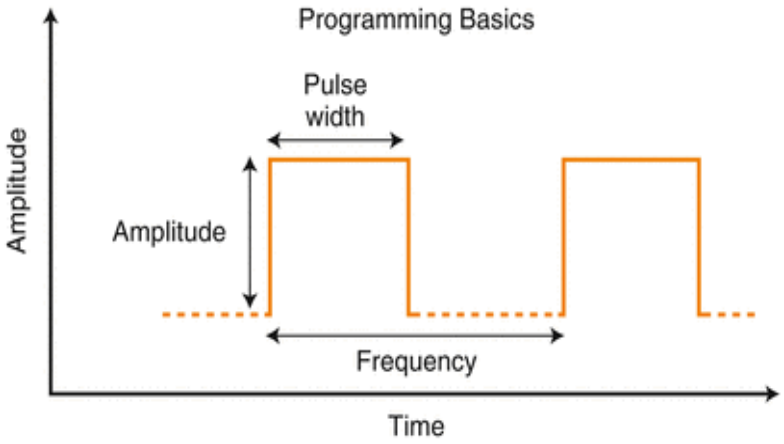

Figure 4: Image and caption modified from [21]. Illustration of tonic stimulation parameters of frequency, pulse width and amplitude.

Figure 6: Image modified from [22]. Image of Spectra Wavewriter IPG manufactured by Boston Scientific (Marlborough, MA). Blue box highlights the connection ports for the stimulator paddle.

Newer stimulator technology has led to the development of implantable pulse generators (IPG) (Fig.5), such as the SPECTRA WaveWriter™ (Boston Scientific, Marlborough, MA), that delivers electrical current to the epidural contacts in a complex waveform at frequencies up to 10 KHz (Fig.6). Although the majority of patients receiving SCS for chronic pain find the paresthetic effect of low-frequency tonic stimulation (LFTS) more tolerable than pain itself, these complex waveforms, known as high frequency burst stimulation (HFBS), have been found to attenuate pain with equal or greater

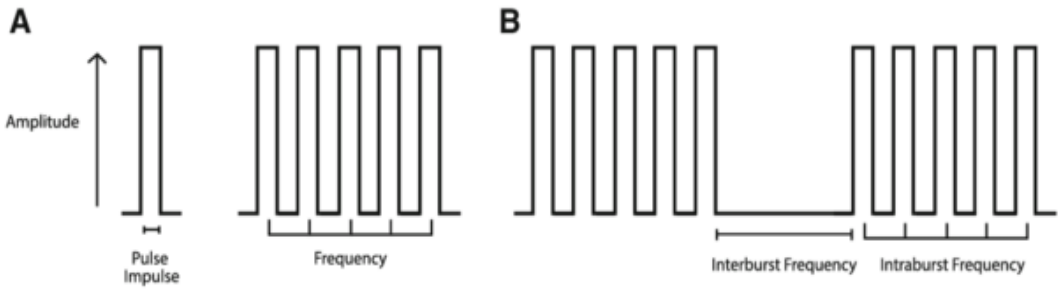

Figure 5: Image and caption modified from [21]. Illustration of SCS parameters for A) tonic stimulation and B) additional parameters for HFBS being interburst frequency and intraburst frequency.

effectiveness without producing paresthesias. In 2015, a large, multi-center, randomized control trial (SENZA-RCT) was conducted to assess the efficacy of high frequency tonic stimulation (HFTS) at 10 KHz using the Senza IPG (Nevro, Redwood City, CA) in patients with chronic pain of the trunk and/or limbs. The trial consisted of 171 subjects receiving surgical placement of an SCS paddle and IPG. Ninety subjects received the 10 KHz-capable IPG and 81 subjects received IPG implants capable of producing traditional tonic stimulation of < 1 KHz. Over 12 months, subjects who received the Senza device experienced stimulation at a frequency of 10 KHz with a 30 μs pulse width and stimulation amplitudes ranging from 1.6 – 3.8 mA, while subjects receiving traditional SCS underwent stimulation at a frequency of 39.2 – 133.5 Hz, pulse widths of 347 – 591 μs and stimulation amplitudes ranging from 3.6 – 8.5 mA. After 12 months of stimulation both groups were assessed for pain relief via Visual Analog Scale (VAS) of 0 / 10, where 10 is severe debilitating pain and 0 is no pain. Subjects receiving 10 KHz stimulation reported a decrease in VAS from 7.4 ± 1.2 to approximately 2.5, a 67% decrease with no reports of paresthesia, whereas subjects receiving traditional LFTS reported a decrease in VAS from 7.8 ± 1.2 to approximately 4.3, a 44% decrease in pain rating ($p < .001$) with all subjects perceiving paresthesias.[23]

Another study investigating efficacy of HFBS for chronic pain was conducted in 2017 by Deer et al, in which 100 subjects participated in a randomized crossover trial (SUNBURST). All subjects that qualified for the study were implanted with the Prodigy SCS IPG manufactured by Abbott (Plano, TX). After surgical placement of the SCS paddle and IPG, subjects were initially programmed with tonic stimulation settings of frequency ranging from 30 – 100 Hz, pulse width of 100 – 500 μs and stimulation amplitudes tailored per each subject according to elicitation of comfortable paresthesias over the region of pain. Subjects were then separated into two treatment groups, where

one group of 45 subjects continued use of tonic stimulation and the other 55 subjects received HFBS with an intraburst frequency of 500 Hz, interburst frequency of 40 Hz, and pulse width of 1 ms delivered in packets of 5 pulses. Each treatment group received their assigned treatment for a total of 12 weeks before the groups were switched to the opposite stimulation type. Following 24 weeks of study, the average amplitude of LFTS was 6.42 ± 4.00 mA while the average amplitude for HFBS was 1.73 ± 1.05 mA ($p < .05$). The primary outcome measure was perceived pain using a 100 mm VAS, where 0 is no pain and 100 is severe debilitating pain. At the end of 24 weeks, a significant difference was found in favor of HFBS with a 5.1 mm difference between HFBS and LFTS regarding VAS rating, and 70.8% of subjects expressed a preference for HFBS over LFTS ($p < .001$).[24] These two important studies highlight the increased capability of advanced waveform SCS to mitigate pain when compared to traditional stimulation parameters.

1.3 Proprioception Signaling

Muscle spindle fibers contain specialized receptors located within skeletal muscle that sense the length and stretch velocity of extrafusal muscle fibers. Proximally, muscle spindles form primary sensory afferents (Ia and II fibers) that project through the dorsal root ganglion (DRG) to the DHSC and then bifurcate, with ventral projections influencing

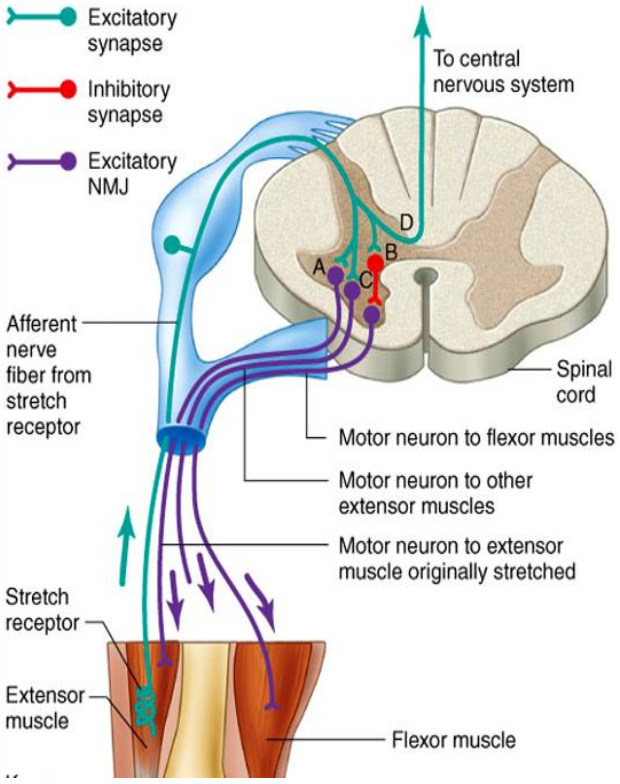

Figure 7: Image and caption modified from [8]. Circuitry diagram of proprioceptive (Ia) signaling leading to A) excitation of homonymous muscle, B) inhibition of antagonist muscle, C) excitation of synergist muscles and D) projection to higher brain centers via dorsal column.

α–motor neurons (Fig.7) and ascending tracts within the dorsal column and posterior spinocerebellar tracts of the spinal cord projecting to nuclei of the medulla and cerebellar cortex respectively. Muscle spindle afferents have been shown to influence α–motor neurons in three ways: 1) monosynaptic excitation, 2) disynaptic excitation and, 3) disynaptic inhibition.[25,26,27]

Golgi tendon organs have receptors located at the insertion of extrafusal muscle fibers with connective tissue of a tendon that sense changes in muscle tension. Primary sensory afferents (Ib fibers) also project through the DRG to the DHSC and then bifurcate, with ventral projections influencing inhibitory and excitatory interneurons and ascending tracts along the dorsal column and anterior spinocerebellar tracts of the spinal cord. The disynaptic effects of Ib fibers on α–motor neurons have been previously studied in humans by Dietz and colleagues using a body weight support crane to reduce load during walking on a treadmill while simultaneously recording surface electromyography (EMG). In healthy controls, reduction in body weight of 50% was shown to cause significant decrease in extensor muscle activation amplitude during late stance when compared to subjects walking with full body weight ($p < .05$).[28] This finding suggests that muscle tension information conveyed by Ib fibers of the golgi tendon organ influences homonymous muscle activation during walking in an excitatory fashion.

Sensory afferent modulation of MN excitability is also facilitated by pain signaling in Aδ fibers, resulting in a withdrawal reflex to noxious stimuli. Withdrawal from cutaneous afferent activation was investigated in 1999 by Andersen et al, where 14 healthy subjects received noxious electrical stimulation on the sole of the foot in 16 different locations while sitting upright. Stimulation was delivered at 1.5x subject pain response threshold according to the visual analog scale (VAS), guaranteeing Aδ fiber recruitment. Surface EMG recording of the gastrocnemius medialis (GM) and tibialis

anterior (TA) muscles along with kinematic changes in ankle position using a goniometer were collected during stimulation. Stimulation of the distal medial sole elicited robust TA activation along with a 6° mean dorsiflexion response, however stimulating the heel region of the sole resulted in GM activation and a 2° mean plantarflexion movement. A significant difference was found between muscle activation ($p < .001$) and kinematic response ($p < .001$) to noxious stimuli delivered to different regions along the sole of the foot.[29] The observations of Andersen and colleagues demonstrate that cutaneous afferent fibers influence MN excitability with modular organization, indicating diverse projections to both excitatory and inhibitory interneurons that may influence motor behavior in someone with chronic pain.

Spaich and colleagues investigated MN response to noxious stimuli during gait. Electrical stimulation, above individual pain threshold, was delivered on the sole of the foot for 15 healthy individuals during 4 different phases of the gait cycle being 1) heel contact, 2) mid-stance, 3) early swing and 4) late swing. Knee angle measurements using a goniometer were continuously recorded during 30 seconds of walking at 3 km/h. The magnitude of knee flexion was found to be significantly smaller from stimuli delivered during the heel contact and mid-stance phases compared to early swing and late swing ($p < .05$).[30] The lack of knee flexion observed during load bearing portions of the gait cycle suggests that withdrawal reflex responses to pain may be modulated, at least in part, by proprioceptive signaling during a functional task. Thus, primary afferent sensory signaling from muscle spindle fibers, golgi tendon organs and Aδ fibers influence α–MNs and interneurons of the VHSC during functional motor tasks, tightly regulating muscle firing to maintain appropriately timed contractions of agonist and antagonist muscles around a joint.

1.4 MUSCLE ACTIVATION PATTERNS DURING GAIT

Persons with neurologic insult due to stroke or incomplete SCI can produce robust activation of individual flexor or extensor musculature in certain experimental conditions. However, in many cases what is lost in these disorders is the ability to produce fine-tuned, integrated movements necessary for dynamic tasks such as walking.[31] A module-based approach to quantify gait patterns was first applied to humans in 2004 by Ivanenko[32], and subsequent work performed in 2010 by Clark et al established that gait could be represented in four modules. The four modules implemented by Clark represent four phases of the gait cycle: 1) Early Stance, 2) Late Stance, 3) Early Swing, and 4) Late Swing.

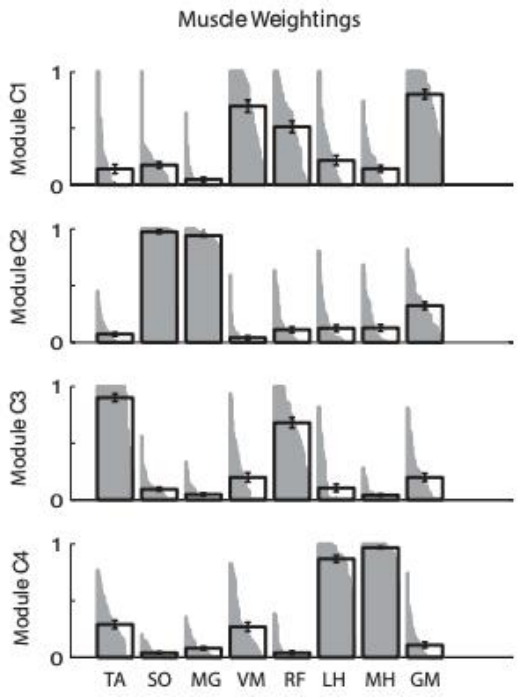

Figure 8: Image and Caption modified from [31]. Illustration of module classifications using groupings of muscle co-activation amplitude (grey shading) during a walking task in 20 healthy subjects with group mean (black box). Muscle weightings are shown for tibialis anterior (TA), soleus (SO), medial gastrocnemius (MG), vastus medialis (VM), rectus femoris (RF), lateral hamstring (LH), medial hamstring (MH) and gluteus medialis (GM).

EMG-based module groupings during a typical gait cycle are illustrated in Figure 8, where early stance shown in module 1 is representative primarily of extensor activity for weight acceptance with activation seen in the vastus medialis (VM), rectus femoris (RF) and gluteus medius (GM). Module 2 represents the late stance phase when plantarflexors are active for forward propulsion, facilitated by muscle activity in the soleus (SOL) and medial gastrocnemius (MG). Module 3, the early swing phase, shows muscle activity primarily in flexors of the hip (rectus femoris or RF) and ankle (tibialis anterior or TA). The late swing phase of the gait cycle, module 4, is during deceleration of the limb for proper foot placement and is facilitated by increased muscle activity in the

medial and lateral hamstrings (MH) (LH). The ability to coordinate timing-dependent muscle co-activations during functional tasks, such as walking, remains dependent, however, on appropriate sensory feedback. Recently, Wagner and colleagues postulated that SCS delivery in a spatio-temporal, rather than tonic, fashion would increase rehabilitation potential in persons with incomplete spinal cord injury due to sparing of important proprioceptive signals by minimizing the amount of time when SCS is on. The spatio-temporal SCS method involves activation of contacts targeting specific posterior nerve roots to recruit musculature facilitating gait in a time-dependent fashion, thus allowing natural sensory afferent signaling to reach the spinal cord when SCS is not needed and inactive. In their study, SCS implantation over the lumbosacral spinal cord (T11 – L2) segments was performed on three male subjects with chronic cervical SCI with severe lower limb deficits. Subjects underwent 15 weeks of assisted over-ground treadmill walking during spatio-temporal LFTS using a dynamic body weight support system. Following 15 weeks of training, subjects performed a walking task during no stimulation, LFTS, and spatio-temporal LFTS with full body kinematic tracking allowing quantification of step height (cm) and walking speed (m/s). A significant increase in step height ($p < .001$) and walking speed ($p < .01$) were found in all 3 subjects during spatio-temporal LFTS supporting their initial hypothesis that primary afferent sensory sparing is fundamental to produce proper gait mechanics. A six-minute walking test was used to assess ambulation recovery following step training with spatio-temporal SCS. One participant increased walking distance from 60 meters to 150 meters while another participant increased from 10 meters to 60 meters. The third participant was unable to complete unassisted walking, however by using a walker he was able to increase walking distance from 0 meters to 300 meters.[33] In a companion study investigating SCS effects on proprioception, Formento and colleagues created a computational model of proprioceptive afferent recruitment in response to SCS. The same model used to

indicate the potential benefit of spatio-temporal LFTS also showed a similar benefit using HFBS at 600 Hz.[3] At the time of these two studies, SCS technology did not allow for testing of HFBS parameters at this frequency.

2.0 MATERIALS AND METHODS

2.1 SCS PADDLE PLACEMENT AND ACTIVATION

This study was approved under IRB protocol # Pro00089881. The subject was consented for placement of a spinal cord stimulator paddle for treatment of chronic low back and leg pain. The subject was informed that during the procedure EMG and SSEP data would be collected and saved at various points during placement. SCS placement was performed using a 32-electrode paddle array (CoverEdge™, Boston Scientific, Marlborough, MA) (Fig.9) implanted at the T7-9 vertebral levels.

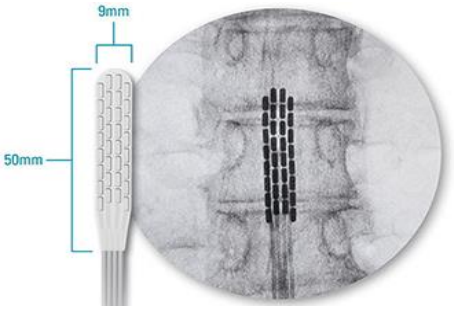

Figure 9: Boston Scientific CoverEdge™ 32 Surgical Lead (left) and fluoroscopic image of the stimulator array after implantation along the dorsal epidural space (right).

The subject was first placed under general anesthesia and positioned prone on the operating room table. Subdermal SSEP and EMG needle electrodes were placed throughout the subject's body by the neurophysiology team as determined by standard of care guidelines.

2.2 SHORT-LATENCY SOMATOSENSORY EVOKED POTENTIAL (SSEP)

SSEP testing of the lower extremities is most commonly performed on the posterior tibial nerve (PTN). Cortical responses to PTN stimulation are recorded using scalp electrodes that are placed according to the 10-20 International System used for electroencephalography (EEG) recordings. Electrodes are placed at CPz (centro-parietal), C3 (left motor cortex), C4 (right motor cortex), and C5 (brainstem). The initial cortical waveform seen during PTN stimulation is a positive deflection approximately 37

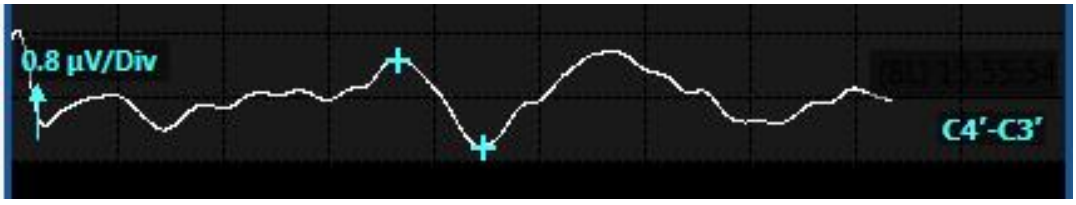

Figure 10: Visualization of baseline SSEP averaging from PTN stimulation recorded between C4-C3 as defined by the 10-20 International System. The two teal crosshair markers represent the P37 (left) and N45 (right) deflections. Waveform represents average response to SSEP stimuli (n = 200).

milliseconds after stimulation (P37), followed by a negative deflection approximately 45 milliseconds after stimulation (N45) (Fig.10).[34] In this study, PTN stimulation and cortical recordings via scalp electrodes were performed using the IOMAX intraoperative neuromonitoring platform (model number 100880-937, Cadwell, Kennewick, WA). Cortical voltage data were sampled at 250 Hz, bandpass filtered between 30 – 500 Hz and responses were averaged every 200 SSEP pulses to calculate averaged waveforms.

2.2.1 SSEP Collision Testing

SSEPs provide a surrogate measure of the sensory activation threshold of dorsal column fibers and can be affected by limb length, body temperature, SCI, spinal stenosis/compression, demyelination and neuropathy. The SSEP latencies described above can also be modulated by SCS through epidural paddle electrodes using a technique known as SSEP Collision Testing. SSEP pulses delivered at a rate of 2.79 Hz with an amplitude of 40 mA will show a decrement of the P37 and N45 deflections as the parameters of the epidural stimuli are altered. To accomplish this, SCS was delivered at a 40 Hz rate with a 300 μs pulse width at a starting amplitude of 1.0 mA and increased in increments of 1.0 mA until SSEP attenuation occurred, which is confirmed by a 100% loss of the P37 waveform.

2.3 Electromyography (EMG)

EMG is used to record motor unit activation. The motor unit is comprised of a single motoneuron (MN) and the muscle fibers innervated by that MN (Fig.11).[35] The muscle fibers innervated by the MN are, like most cells, semi permeable structures tightly regulated via

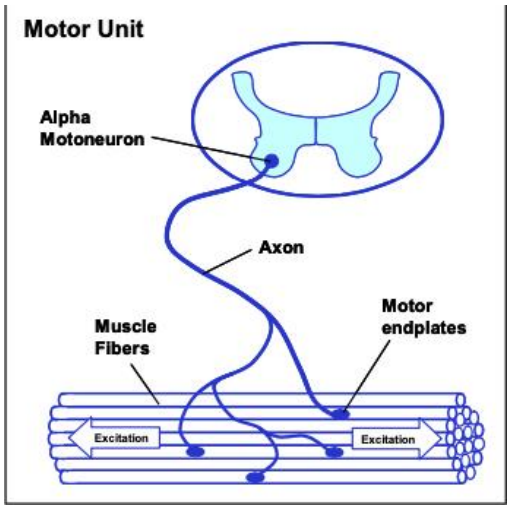

Figure 11: Image and caption adapted from [35]. Illustration of a single Motor Unit.

voltage-gated ion channels that at rest allow for flow of potassium (K^+) ions out of the membrane and restriction of sodium (Na^+) ions from entering the cell, resulting in a membrane potential of ~ -80mV.

When a lower MN is activated, the neurotransmitter acetylcholine (ACh) is released from motor endplate presynaptic terminals, facilitating conformational changes in the voltage-gated channels of muscle fibers leading to Na^+ influx and rapid depolarization. The wave of depolarization along a group of coactivated muscle fibers forms an electric dipole and, with the application of bipolar electrodes placed on the skin, underlying muscle activity can be captured as a potential difference in voltage between the electrodes. Illustrated in Figure 12, a wave of depolarization moves along the muscle fibers along several time points (T1-T5), where sensing electrodes, outlined in green boxes, connected to an amplifier record the potential difference (blue sinusoid) in samples of voltage, resulting in both positive and negative deflections in the EMG of equal amplitudes.

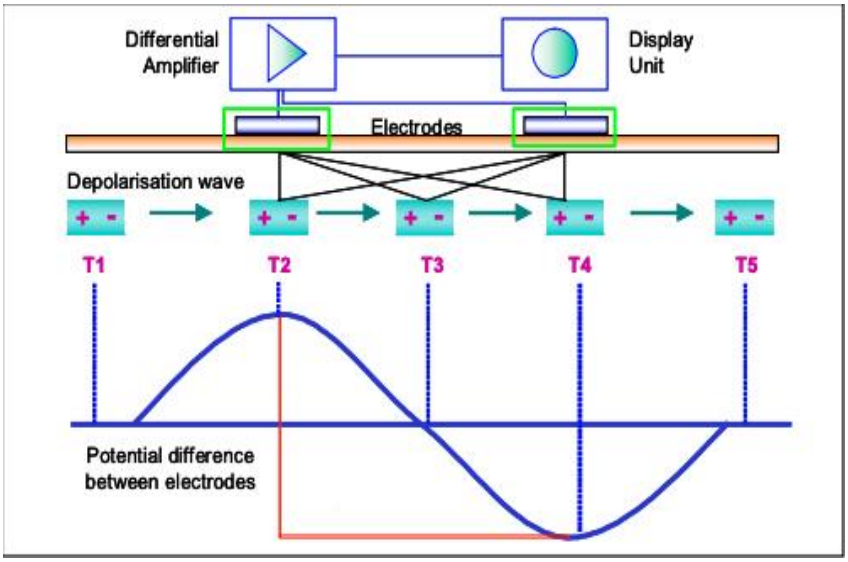

Figure 12: Image and caption modified from [35]. EMG electrode setup used to capture electrical signals from underlying muscle tissue.

2.3.1 EMG Recording During SCS Activation

In the present study, we performed epidural paddle stimulation while monitoring EMG activity. The SCS parameter used were the same LFTS parameters found to attenuate the P37 and N45 deflections during the aforementioned SSEP collision testing.

Following LFTS, two other parameter settings were tested at the same amplitude including: HFBS with 600 Hz intraburst / 40 Hz interburst and HFBS with 1200 Hz intraburst / 40 Hz interburst (Fig.13).

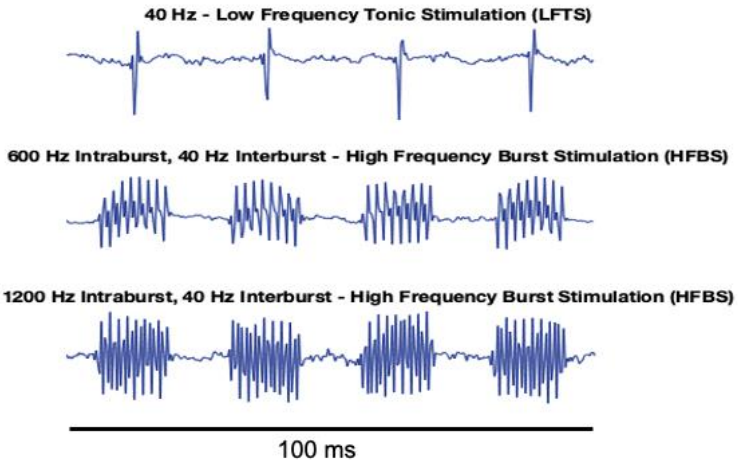

Figure 13: Visualization of EMG tracings during different SCS stimulation parameters. Illustration is derived from stimulator artifact captured via subdermal needle EMG electrodes placed in the Rectus Abdominus.

EMG was collected intraoperatively using 13 mm stainless steel subdermal needle electrodes (model # RLSP310, Rhythmlink International, Columbia, SC) at a sampling rate of 3 kHz using a 16-channel recording device (LR10™, Tucker Davis Technologies, Alachua, FL) that served as a signal amplifier and analog-to-digital converter. EMG was recorded bilaterally from three lower extremity muscles (Vastus Lateralis (VL), Tibialis Anterior (TA), Soleus (SL)) and rectus abdominus muscles to allow for visualization of stimulator artifact (Fig.14). During extraoperative EMG measurements, 15 x 20 mm conductive vinyl surface EMG self-adhesive electrodes (model # PSTCUL15026, Rhythmlink International, Columbia, SC) were placed on the skin over the same muscles tested intraoperatively.

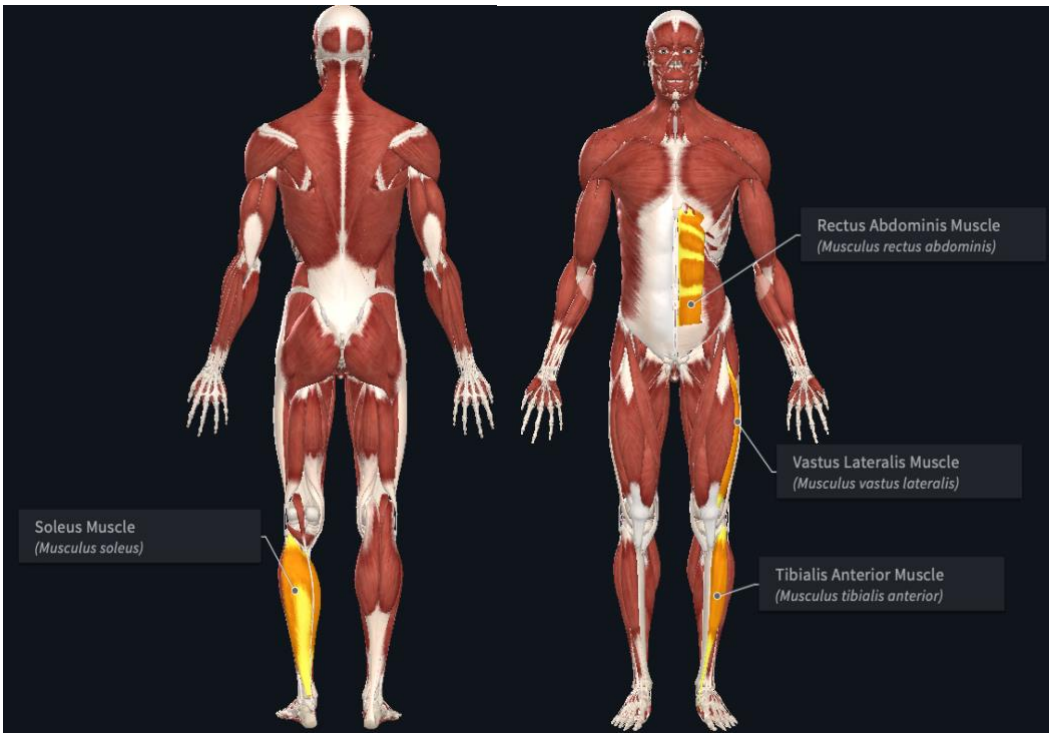

Figure 14: Visualization of musculature chosen for EMG recording during SCS activation.

Following intraoperative testing, the subject was given at least 30 days to recover before being asked to return for further extraoperative SCS testing using surface EMG as described above. Given that during intraoperative procedures the subject was placed under general anesthesia, performing extraoperative SCS allowed for feedback regarding sensory thresholds and quality of pain reduction from LFTS and HFBS parameters. Extraoperative EMG recording was performed at perceived sensory threshold, 1.5x perceived sensory threshold and 2x perceived sensory threshold for each SCS parameter tested. Perceived sensory threshold was established by increasing SCS amplitude in increments of 1.0 mA per parameter set until the subject verbally reported sensation of the stimulation. Perceived sensory threshold measurements and surface EMG were collected while the subject was awake and side-lying.

2.3.2 EMG PROCESSING AND ANALYSIS

EMG signals at rest (both intra- and extraoperative) were high-pass filtered above 10 Hz (MATLAB®, Mathworks, Natick, MA). The frequency of an EMG signal typically ranges from 0 – 500 Hz, however true muscle activity may be hard to visualize without application of a filter. A 10 Hz high-pass filter is commonly used to attenuate noise from background muscle activity. Voluntary movement and movement of the EMG leads can also contribute significant noise. Although the subject was under general anesthesia during intraoperative SCS testing, noise below 10 Hz was observed in the signal presumably from the movement of EMG leads and the use of a compression cuff on each leg during surgery to prevent blood clots. Therefore, EMG signals recorded during intraoperative and extraoperative SCS were filtered in the same manner. All EMG data collected at rest were resampled to 1 KHz.

Once the subject completed both intraoperative and extraoperative SCS sessions with EMG recording, peaks in the EMG time series were examined for evoked potentials, which typically has a tri-phasic response (Fig.15). Evoked potential peaks in the time series were identified as a positive deflection in the EMG of at least 30 μV from

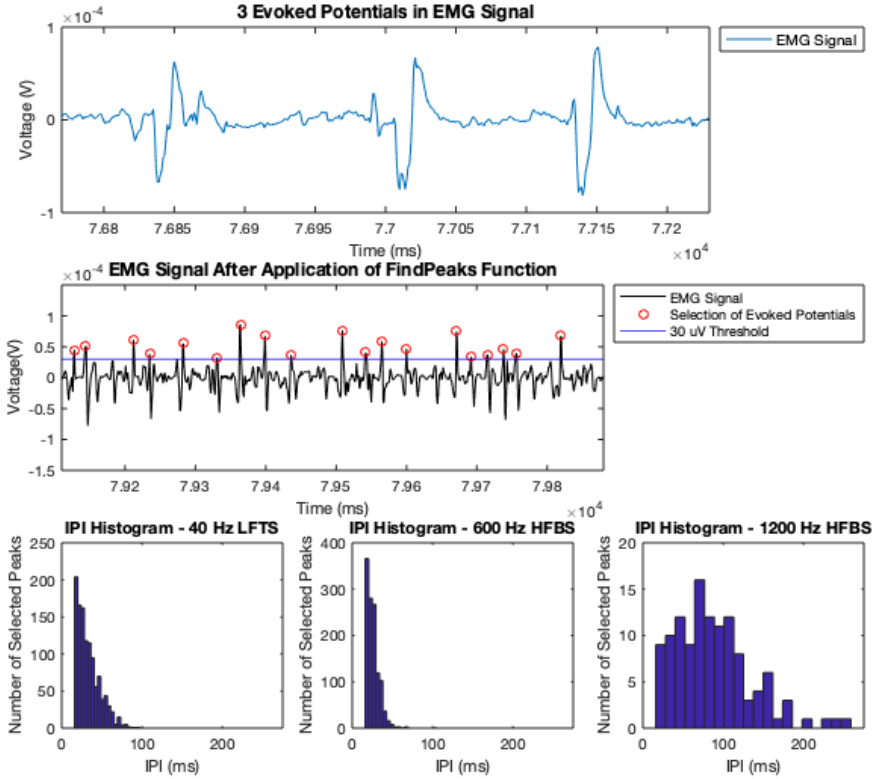

Figure 15: Illustration of Top) evoked potentials in EMG signal, Middle) selection of evokec potential peaks (red circles) with positive deflections reaching threshold (blue line) and, Bottom) IPI histogram of selected potentials.

baseline.[34] Figure 16 illustrates several examples of evoked potentials in the EMG signal (top) identified by our algorithm (middle). The signal in each channel was assumed to arise from a single source. This is confirmed using a histogram of the interpeak intervals as shown in the bottom panel.

2.4 PROPRIOCEPTION TESTING

We investigated the perceived change in knee joint angle and direction of movement reported by the subject using a Threshold to Detect Passive Movement (TTDPM) task (System 4 Pro™, Biodex Medical Systems, Shirley, NY).[3,35] The TTDPM protocol, which utilizes an isokinetic/isometric dynamometer, began with the subject sitting in the Biodex testing seat and the tested leg strapped to the rotating arm of the dynamometer at the lower shank with the non-tested leg resting with approximately 90° of knee flexion (Fig.16). In order to prevent the subject from witnessing initiation, direction and approximate distance traveled of the shank, the subject wore a blindfold and headphones playing a pink background noise. Pink noise is defined as noise in which the power spectral density of the signal is inversely proportional to the frequency, thus the amount of energy is consistent along all frequencies. Pink noise is bandpass filtered between 20-20,000 Hz and is designed specifically to mask electrical noise produced by the Biodex dynamometer.

Figure 16: Image and caption modified from [35]. Illustration of the TTDPM using a Biodex Dynamometer

The TTDPM consisted of at least 10 trials for each stimulation condition, with the dynamometer moving at a rate of 1°/second in a randomized flexion / extension direction. The subject controlled a handheld switch that immediately halted movement of the dynamometer arm, which was to be activated once the subject perceived movement or if the subject began to feel any pain or discomfort throughout the task. Once the dynamometer arm was stopped, the change in knee angle was recorded by the Biodex software. The subject in this study reported discomfort during passive right hip flexion, therefore TTDPM testing was only performed on the left leg. The SCS paddle was activated along the leftmost column of contacts on the epidural paddle, with the bottom left contact selected as the anode (+) and the superior 7 contacts equally distributed as cathodal (-) contacts. Both LFTS and HFBS over the chosen contacts produced paresthesias in reported areas of the patient's chronic pain in the left leg, thus the subject was blinded to stimulation modality. SCS amplitudes were identified during sensory threshold testing, and 1.5x sensory threshold was chosen as the experimental amplitude for each parameter set due to the potential for discomfort with higher stimulation amplitudes during prolonged testing.

2.5 WALKING TASK AND MODULE CLASSIFICATION

Figure 17: Subject fitted with LED markers during walking task.

Following proprioceptive testing, the subject performed a walking task at the 800 sq. foot Locomotor Energetics & Assessment Laboratory at the Medical University of South Carolina (MUSC). A thoracic harness (model # M120, Robertson Mountaineering, Fort Collins, CO) anchored to the ceiling over the floor-mounted treadmill (FIT, Instrumental Treadmill, Bertec, Scotland, U.K) was used to safeguard against a potential fall (weight limit = 300 lbs). Vertical ground reaction forces were recorded from

the treadmill in order to determine gait cycles, where heel strike and toe off were thresholded at 20 newtons or greater. Kinematic tracking was performed using LED markers placed over 64 anatomical regions of interest (Fig.17), allowing a 16-camera motion capture system (Impulse, PhaseSpace, San Leandro, CA) mounted throughout the room facing the treadmill to collect time-stamped positional data throughout the task. Marker coordinates were recorded at 120 Hz. The orientation of each tracked segment was obtained through a least-squares approach by matching the marker locations in the segment's reference frame to the marker coordinates in the global reference frame. The pose of segments with less than 3 visible markers could not be calculated. Surface EMG (model DE 2.1, DELSYS Incorporated, Natick, MA) using 99% silver electrodes was recorded bilaterally from the gluteus medius, semimembranosus, biceps femoris, vastus medialis, rectus femoris, tibialis anterior, soleus and medial gastrocnemius. EMG was sampled at 2,000 Hz using a 32-channel recording device (MA300 system, Motion Labs, Baton Rouge, LA) and high pass filtered at 40 Hz. Observed EMG signals recorded during walking exhibited higher degrees of noise from dynamic movement, therefore a larger high pass filter than that used for EMG data collected during SCS testing at rest was used.

The subject was asked to walk at a normal pace for one minute per tested condition, with the initial 10 seconds being used to optimize steady-state walking conditions and the remaining time to be used for capture of at least 10 consecutive steady state gait cycles. Trials included baseline recording during gait with no SCS stimulation, 600 Hz HFBS with a 40 Hz inter-burst and 140 μs pulse width, and 40 Hz LFTS with a 140 μs pulse width. Both SCS parameters tested were applied at their respective 1.5x sensory threshold amplitudes found prior to proprioception testing.

Segments of EMG recorded during walking at self-selected walking speed were used to investigate complexity of muscle synergies using a nonnegative matrix factorization (NNMF) algorithm (MATLAB®, Mathworks, Natick, MA). The approach illustrated in figure 18 involves calculation of an mxt matrix of the original EMG data (EMG_0), where m represents the number of muscles being measured and t represents a time base normalized to percentage of gait cycle. The algorithm also calculates two surrogate matrices, mxn and nxt, where n is the amplitude of muscle activation.[31] The product of the surrogate matrices are considered a reconstruction of EMG (EMG_r). EMG_r for each module is then compared to EMG_0 by finding the variability accounted for (VAF) (Equation 1).

$$(VAF = 1 - [EMGo - EMGr]^2/EMGo^2)$$

VAF was applied for all 8 eight muscles and across 6 phases of the gait cycle (1 - first double support, 2 - first half of ipsilateral single leg stance, 3 - second half of

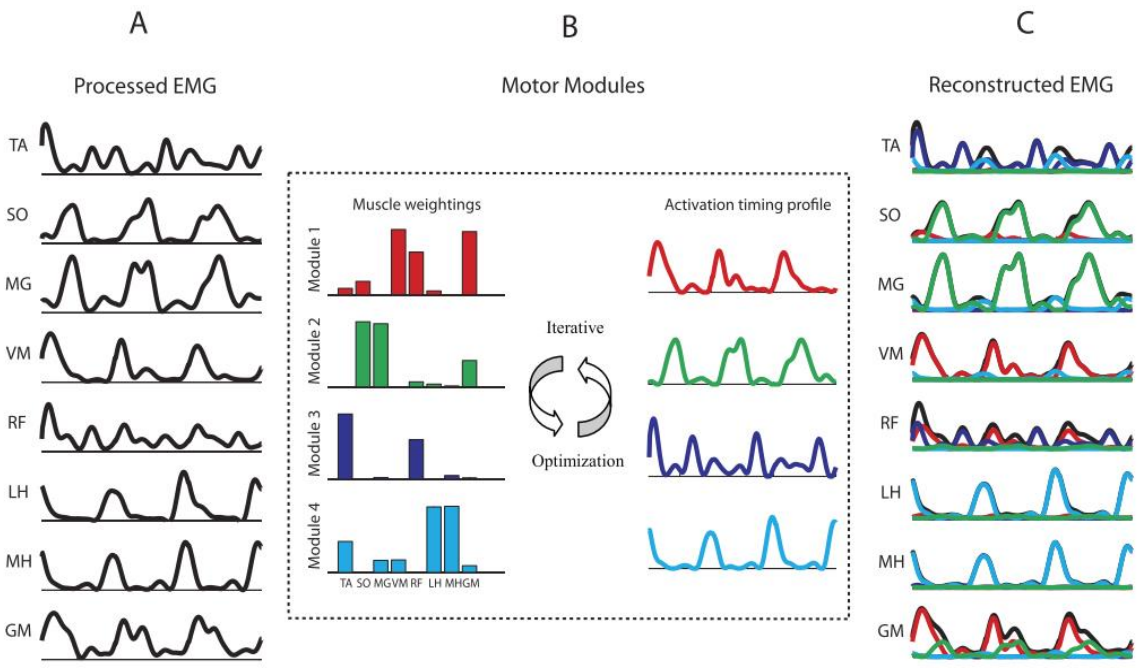

Figure 18: Figure taken from Clark et al [29]. Illustration of the NNMF process over three gait cycles where A) is the original EMG, B) shows the iterative NNMF process where muscle activation timing profiles and muscle activation amplitudes are reconstructed to closely resemble the original EMG and C) the summation of motor modules represent the final reconstructed EMG signal.

ipsilateral single leg stance, 4 - second double support, 5 - first half of ipsilateral swing, 6 - second half of ipsilateral swing), where a threshold necessary for module classification was chosen to be 90% for all 14 conditions (8 muscles + 6 phases of gait) based on similar studies in the literature.[31,38] Classifications were not increased unless the higher module VAF was at least 5% higher than the preceding module. In Clarke's study, the lowest EMG moduling complexity was 2 and represents a gait pattern characterized by high tone throughout the lower extremities and dominated by the stance and swing phases. The gait pattern of these individuals is severely impaired. An EMG moduling complexity of 4 represents normal gait pattern and muscle activations.

2.6 Statistical Analysis

All statistical tests were performed using (MATLAB®, Mathworks, Natick, MA). Data were tested for normality using an Anderson-Darling normality test. For aim 2, a non-parametric Kruskal-Wallis test was used to compare EMG amplitude and interpulse interval (IPI) during extraoperative SCS testing to determine sensory threshold. We compared three groups: 40 Hz LFTS, 600 Hz HFBS and 1200 Hz HFBS. Also for aim 2, TTDPM values were analyzed using a one-way ANOVA to compare data recorded during no stimulation, HFBS and LFTS. In aim 3, step height data collected during the walking task were analyzed using a one-way ANOVA to compare effects from no stimulation, HFBS and LFTS. All error bars and shading represent standard error.

3.0 RESULTS

Our study involved a 74-year-old male subject with chronic neuropathic pain of the lower back and bilateral legs (left worse than right). The subject was previously diagnosed with lumbar radiculopathy and had undergone multiple thoracic spine surgeries. Pain severity was rated at 8 / 10 on a Numeric Rating Scale (NRS) ranging from 0-10 with 0 being no pain and 10 being severe disabling pain. The patient had failed conservative measures, including physical therapy. He was referred to Dr. Rowland for evaluation for spinal cord stimulator. He underwent a full neuropsychological evaluation which judged him to be cognitively competent for the procedure. The patient was informed of and consented to the research protocol. SCS placement was performed using a 32-electrode paddle array (CoverEdge™, Boston Scientific, Marlborough, MA) implanted at the T7-9 vertebral levels, confirmed via intraoperative fluoroscopy.

3.1 EMG RESPONSE DURING INTRAOPERATIVE SCS

SSEP collision testing during SCS was performed in order to ascertain the SCS amplitude needed during 40 Hz LFTS to recruit underlying Aβ fibers. SCS stimulation began at 1.0 mA and increased in increments of 1.0 mA until attenuation of both P37 and N45 waveforms was witnessed via live recordings of cortical deflections using the IOMAX stimulation and recording system. A stimulation amplitude of 4.0 mA was found to be necessary for SSEP attenuation, shown in figure 19, in which the baseline cortical responses are represented in white and cortical responses during SCS in purple.

Using the SCS amplitude of 4.0 mA from SSEP collision testing, multiple SCS parameter types were then tested while recording EMG from lower extremity muscles. Three

Figure 19: Cortical activity showing P37 and N45 waveforms during SSEP baseline testing (white) and during SSEP collision testing using 40 Hz LFTS at an amplitude of 4.0 mA (purple). Waveforms represent average response to SSEP stimuli (n = 200).

stimulation parameters were chosen: LFTS - 40 Hz, 300 µs, 4.0 mA, HFBS - 600 Hz intraburst, 40 Hz interburst, 300 µs, 4.0 mA and HFBS - 1200 Hz intraburst, 40 Hz interburst, 140 µs, 4.0 mA. LFTS at 40 Hz was chosen due to its high prevalence of use for both pain mitigation and motor rehabilitation studies. HFBS at 600 Hz was selected based on the hypothesis by Formento and colleagues that 600 Hz HFBS would optimally preserve proprioceptive information based on primary afferent modeling.[3] HFBS at 1200 Hz was also selected for testing due to the SCS system having a max frequency capability of 1200 Hz.

Change in baseline EMG activity was observed during HFBS using a frequency of 600 Hz intraburst, 40 Hz interburst, 300 µs pulse width

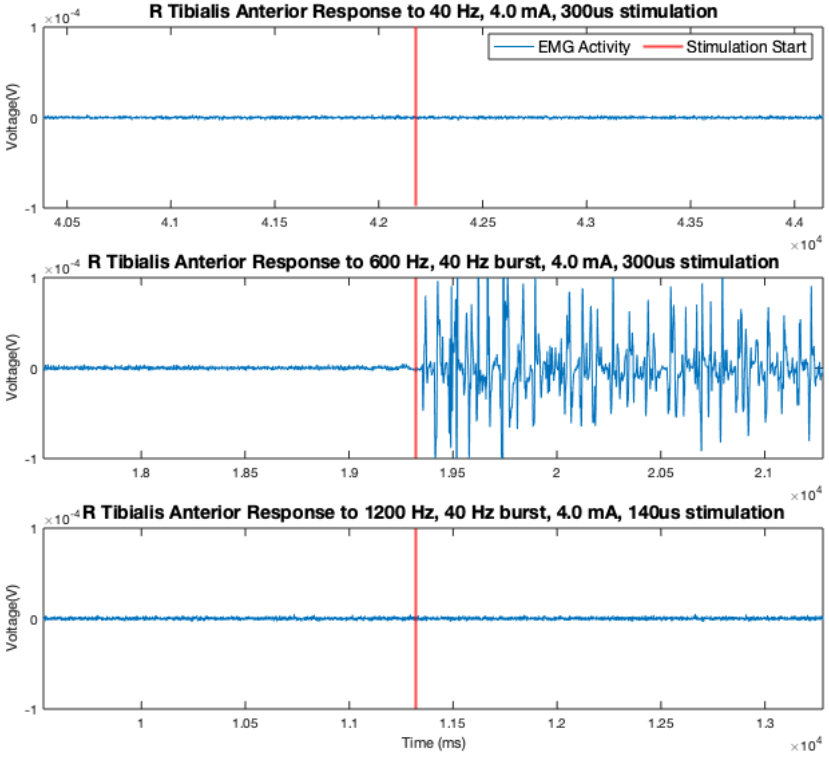

Figure 20: EMG response in Right Tibialis Anterior to varying SCS parameters at 4.0 mA. The onset of stimulation is represented with a red vertical line.

and amplitude of 4.0 mA. Figure 20 shows filtered EMG responses from the right TA to 40 Hz LFTS, 600 Hz HFBS and 1200 Hz HFBS. Voltage amplitudes of EMG response are represented along the Y-axis while time is along the X-axis, where the red vertical line indicates the start of SCS for each parameter set. Although EMG responses to right tibialis anterior are shown, robust changes in EMG activity were observed in all recorded musculature on the ipsilateral side of stimulation using the 600 Hz HFBS only.

3.2 EMG RESPONSE TO SCS DURING SENSORY TESTING

Following thirty days of recovery, the subject returned for further SCS testing in which subjective feedback could be documented. Sensory threshold testing (i.e., increasing SCS intensity until the subject perceives the stimulation) was performed with similar SCS parameters used during intraoperative testing and are shown in Table 1 below.

Table 1: SCS parameters used for later EMG testing and corresponding amplitude necessary for subject to perceive stimulation

Stimulation Type / Pulse width	Perceived Sensory Threshold Amplitude (mA)
40 Hz, LFTS / 140 μs	9.6
600 Hz, HFBS, 40 Hz interburst / 140 μs	3.7
1200 Hz, HFBS, 40 Hz interburst / 140 μs	2.8

Although the stimulation types used during intraoperative investigation remained constant, both 40 Hz LFTS and 600 Hz HFBS had pulse width standardized to 140 μs to more accurately compare effects among the different parameters. The subject reported equal amounts of pain reduction among all three parameter types at the 1.5x perceived sensory threshold level. Using information obtained during extraoperative perceived sensory threshold testing, we measured EMG responses to each parameter tested. SCS

amplitudes were increased from sensory threshold, to 1.5x sensory threshold and up to 2.0x sensory threshold (beyond which the subject reported discomfort). EMG analysis was performed on signals recorded at the 2.0x sensory threshold amplitude.

Figure 21 shows filtered EMG activity from the left soleus during individual parameter testing of 40 Hz LFTS, 600 Hz HFBS and 1200 Hz HFBS, where EMG voltage is represented along the Y-axis and time along the X-axis. Superimposed over the raw EMG is a green vertical line showing the start of 1.5x sensory threshold SCS, a red line showing when stimulation amplitude reached 2x sensory threshold and a blue box outlining the region of EMG analyzed for statistical testing. Mean amplitude analysis of selected EMG showed greater activation in response to 600 Hz HFBS when compared to 40 Hz LFTS and 1200 Hz HFBS ($p < 0.001$, Kruskal-Wallis test). Evoked potentials were not observed in the EMG data of either vastus lateralis or tibialis anterior muscles during 1200 Hz HFBS, therefore no statistical analysis were performed comparing those groups. In Table 2, the mean amplitude of evoked potentials

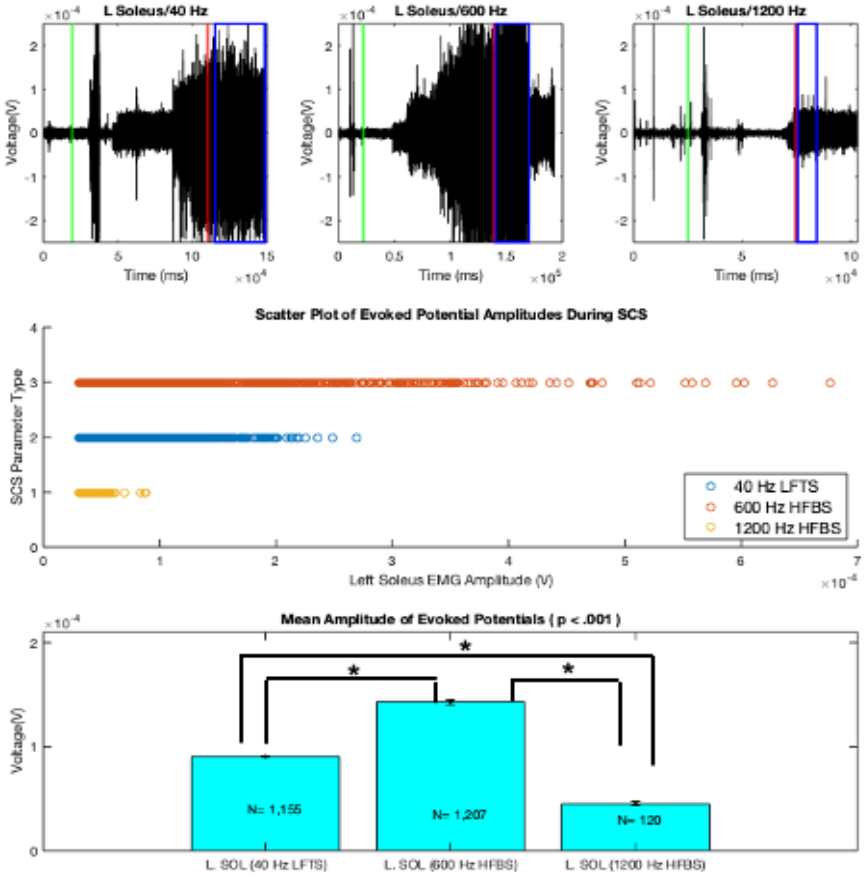

Figure 19: Analysis of evoked potentials where Top) shows filtered EMG response to SCS, Middle) a scatter plot of amplitude data for selected evoked potentials and, Bottom) mean amplitude of selected potentials with standard error. * (p < .001, Kruskal-Wallace)

for all muscles recorded along with mean interpeak interval calculated during HFBS and LFTS testing are shown along with corresponding p-values.

Table 2: Data collected during SCS testing at 2.0x sensory threshold with evoked potential amplitude, IPI and corresponding p-values shown.

Muscle	Stimulation Type	SCS amplitude (mA)	mean amplitude (microvolts)	p-value	mean IPI (ms)	p-value
Group 1						
Vastus Lateralis (VL)	40 Hz, LFTS	19.2	33.7 ± 0.7	< .01	302.6 ± 11.3	< .01
VL	600 Hz, HFBS, 40 Hz interburst	7.4	122.1 ± 2.5		54.4 ± 1.3	
Group 2						
Tibialis Anterior (TA)	40 Hz, LFTS	19.2	39.2 ± 0.8	< .01	296.1 ± 71.1	< .01
TA	600 Hz, HFBS, 40 Hz interburst	7.4	69.7 ± 0.9		54.5 ± 0.3	
Group 3						
Soleus (SOL)	40 Hz, LFTS	19.2	90.4 ± 1.2	< .01	33.5 ± 0.4	< .01
SOL	600 Hz, HFBS, 40 Hz interburst	7.4	143.0 ± 2.6		25.4 ± 0.2	
SOL	1200 Hz, HFBS, 40 Hz interburst	5.6	44.9 ± 1.9		87.7 ± 4.4	

3.3 Differences in Passive Motion Detection

Due to prolonged SCS activation at 2.0x sensory threshold, the TTDPM test was completed using stimulation amplitudes at 1.5x sensory threshold for the 40Hz LFTS and 600 Hz HFBS parameters. Figure 22 shows results of the TTDPM among the three testing conditions being 1) no stimulation, 2) 600 Hz intraburst, 40 Hz interburst, 140 μs, 7.4 mA and, 3) 40 Hz, 140 μs, 14.4 mA. Results from a one-way ANOVA test for the 10 trials per tested condition indicate a non-significant difference between no stimulation and the HFBS parameter set, with a significant difference existing between LFTS and the other two testing conditions ($p < .001$).

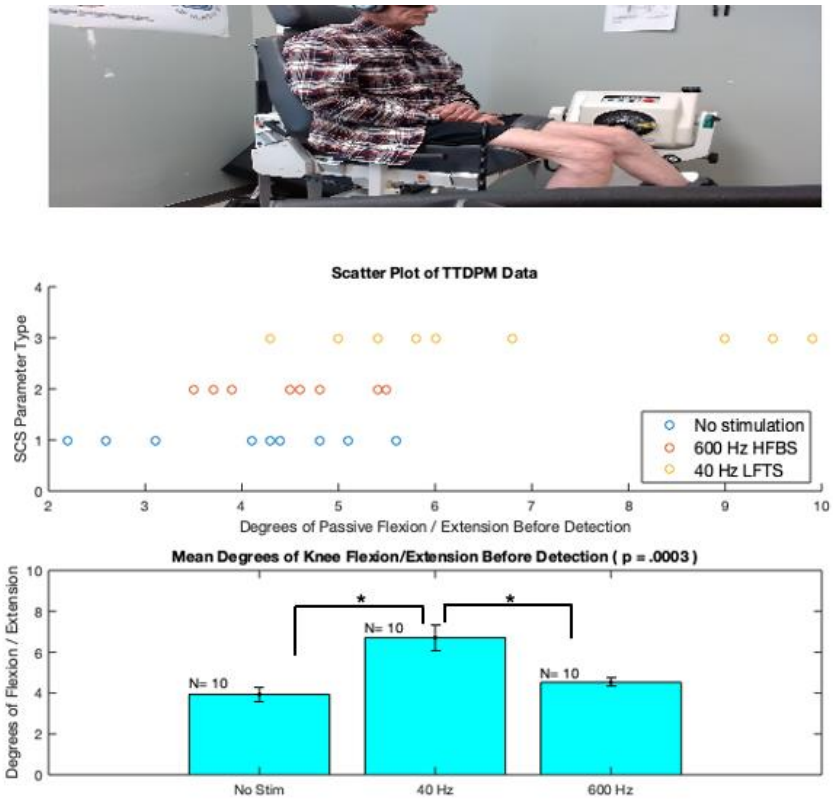

Figure 20: Results from the TTDPM showing, Top) illustration of the TTDPM testing process, Middle) a scatter plot of recorded degrees of passive flexion/extension before detection and Bottom) mean degrees of knee flexion/extension passively applied before subject recognizes movement. * ($p < .001$, One-way Anova)

3.4 Differences in Module Classification and Kinematics

Muscle activation patterns and kinematic features observed during gait can be quantified by a measure known as EMG moduling complexity. We compared EMG

moduling complexity in our subject in response to no stimulation, 40 Hz LFTS and 600 Hz HFBS (performed at 1.5x sensory threshold for each stimulation parameter).

Figure 23 displays the muscle weightings among the 4 classified modules, corresponding to the 4 components of the gait cycle identified by Clark: early stance, late

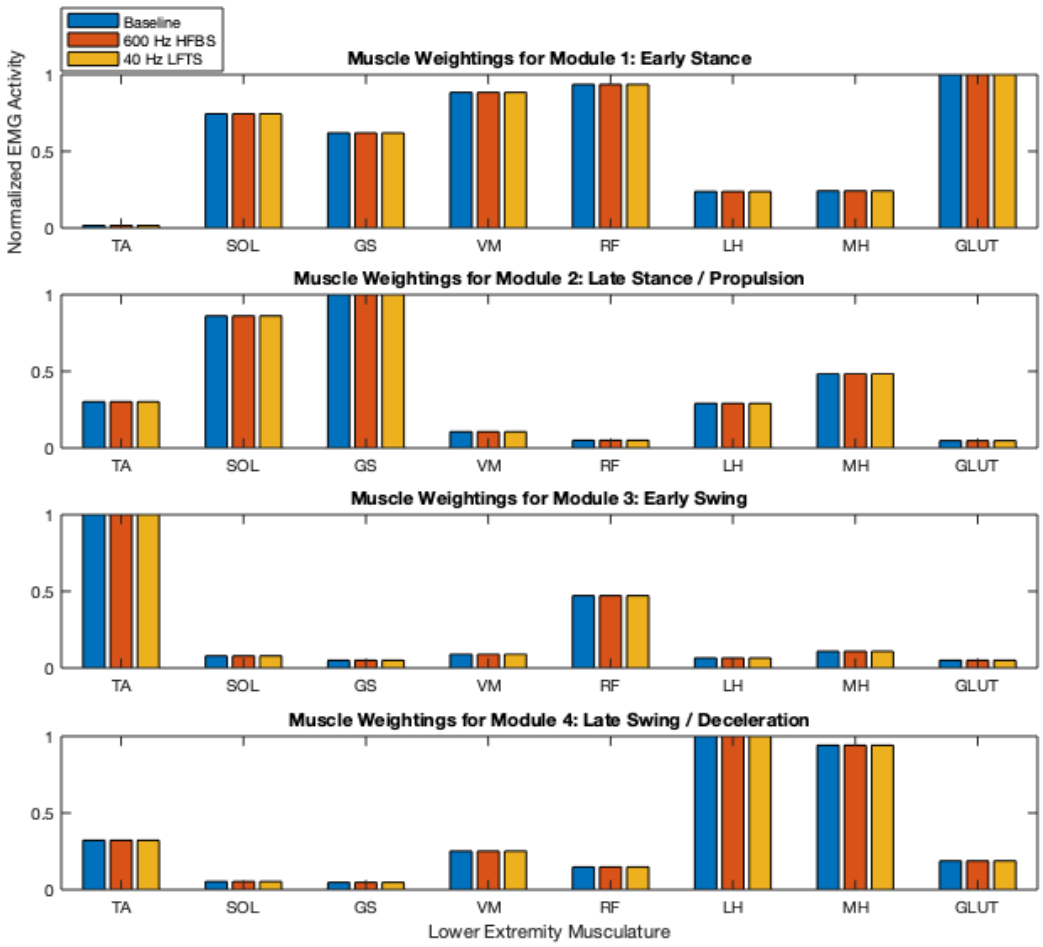

Figure 21: Results from EMG module classification showing muscle activation patterns among various testing conditions where it may be seen that muscle co-activations during functional task are similar

stance, early swing and late swing. EMG was normalized to the highest activated muscle (value of 1.0). Normalized EMG amplitudes per module are located along the Y-axis, while individual muscles (i.e., channels) are located along the X-axis. The classification of EMG modules (See 1.6, 2.4) was found to have no change among the tested conditions of 1) no stimulation, 2) 600 Hz intraburst, 40 Hz interburst, 140 μs, 7.4 mA

and, 3) 40 Hz, 140 μs, 14.4 mA. All parameters tested resulted in a module complexity classification of 4 modules, which represents the highest moduling complexity.

Although EMG activity during walking did not deviate among the tested conditions in large enough amounts for the NNMF algorithm to differentially assign module classification, further investigation of the raw EMG during walking showed observable differences in muscle firing among the different SCS trials and baseline testing. Figure 24 shows EMG amplitude (Y-axis) of left TA averaged across all completed gait cycles (normalized by percentage of the cycle) for each stimulation parameter tested, where TA activity during HFBS (blue) more closely resembles TA activity during no stimulation (green) than TA activity during LFTS (red) throughout most of the cycle. Specifically, between 50 and 60 % of the gait cycle, the pre-swing phase is where TA activity should be minimal allowing proper plantarflexion and propulsion. [39] Figure 24 shows results in line with this estimation. Baseline gait EMG signal amplitude falls dramatically during this interval, as does the amplitude during HFBS but not LFTS.

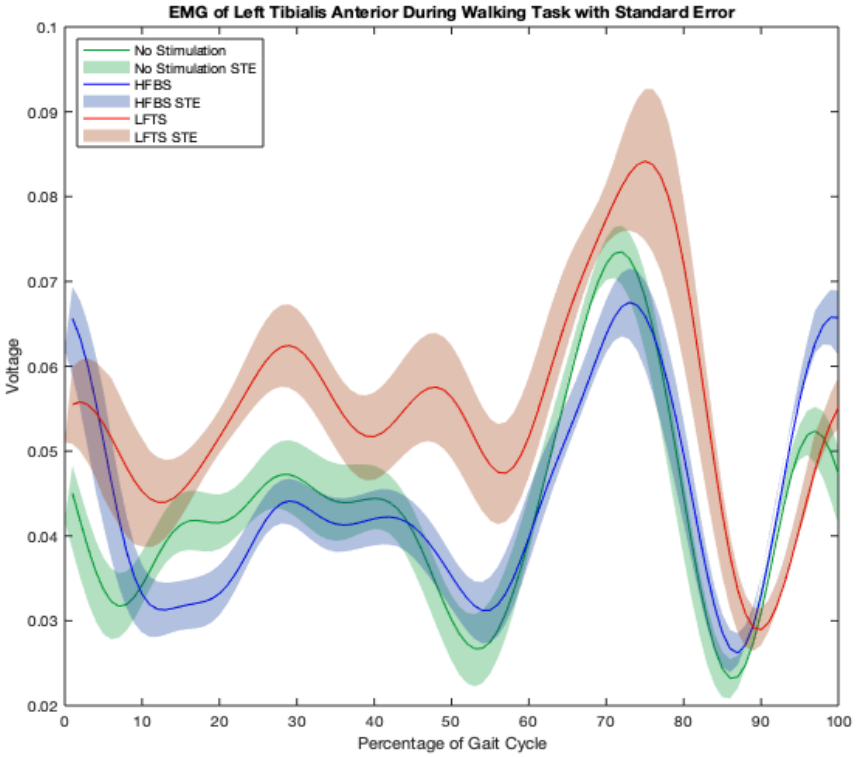

Figure 22: EMG recorded from the left tibialis anterior through each testing condition. EMG signal is average of all gait cycles during each tested condition.

Regarding gait kinematics, significant difference was observed in step height for both the left and right foot, with HFBS more closely resembling baseline height for the left and right side. Figure 25 shows the gait cycle beginning with right heel strike at 0% and ending with the next recurring right heel strike at 100%, where a red box has been placed around the mid-swing phase at approximately 80% of the gait cycle where foot height should reach a maximum.

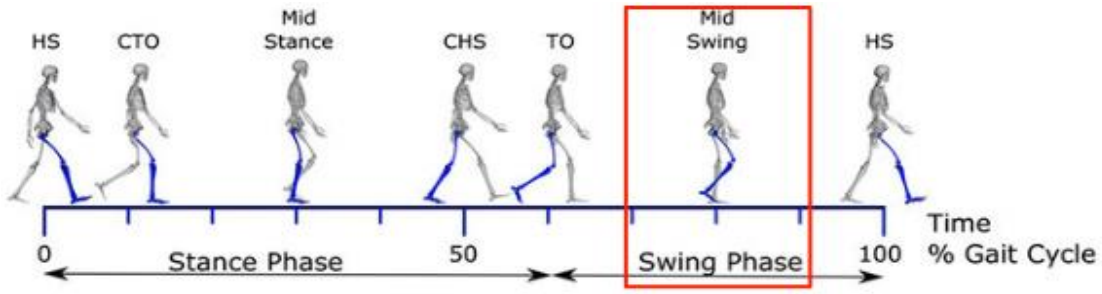

Figure 23: image a caption modified from [40]. Illustration of appropriate kinematics during the gait cycle

Figure 26 shows several traces of foot height in meters (Y-axis) over 100% of the gait cycle (X-axis) during no stimulation (baseline), HFBS and LFTS averaged over all completed gait cycles with shaded regions representing standard error. A non-significant difference, using a one-way ANOVA,

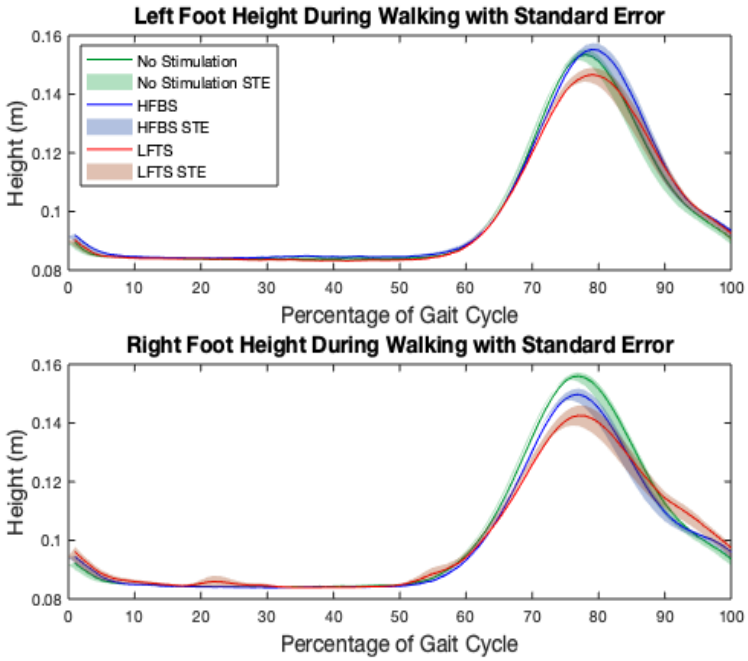

Figure 24: Height measurement during gait in meters of the Top) left foot with standard error and, Bottom) right foot with standard error.

exists between baseline testing conditions and trials during HFBS ($p > 0.05$), and a significant difference exists between baseline conditions and trials during LFTS with a p-value of $< .05$ and $< .01$ for left and right foot height, respectively.

4.0 DISCUSSION

Results from SCS parameter testing during intraoperative stimulator placement under general anesthesia, awake sensory threshold testing at rest during EMG recording and dynamic walking task during EMG and motion capture suggest that HFBS and LFTS differ in several important aspects. Specifically, 600 Hz HFBS may have the unique capacity to influence motor pathways of the spinal cord without significantly disrupting sensory afferent signaling or significantly impacting movement dynamics during a functional task. This could be an important advance in the motor rehabilitation field if this result can be replicated in more patients with chronic pain and motor deficits, because it points to a possible mechanism of selective sparing of proprioceptive input when engaging motor tasks.

Observations made during intraoperative testing show that LFTS at amplitudes necessary to recruit Aβ fibers, seen during the SSEP collision protocol, are not sufficient enough to recruit lower motoneurons (MN) of the ventral horn of the spinal cord (VHSC). This was also true at the maximum device stimulation frequency of 1200 Hz, regardless of burst or nonburst stimulation pattern. In contrast, 600 Hz HFBS produced robust and sustained activity in the EMG from all three lower extremity muscles indicating the ability to influence downstream targets of the VHCS across multiple spinal levels. The ability of 600 Hz HFBS to accomplish this task, and the inability of 40 Hz LFTS, may be due to the ability of neurons to interpret multiple small amplitude stimuli in high frequency as one large stimulus given in a single pulse. While the principle of temporal summation may be able to account for the difference in HFBS and LFTS, it would not necessarily explain why 600 Hz HFBS and 1200 Hz HFBS do not produce similar results.

One possible explanation for the difference between 600 Hz and 1200 Hz HFBS to recruit VHSC motoneurons might be a phenomenon known as synaptic fatigue, where rapid stimuli producing fast trains of action potentials lead to a decay in post synaptic

activity, which in this case might implicate the role of interneurons located within the superficial dorsal horn of the spinal cord (DHSC). Synaptic fatigue is generally thought to occur due to an inability to endocytose vesicles containing neurotransmitters in a rapid enough fashion to entrain excitation to neighboring post synaptic densities. However, it should also be noted that limitations in stimulator technology did not allow for 1200 Hz HFBS to be delivered with a 300 μs pulse width, which was used during 600 Hz HFBS, and instead was restricted to a 140 μs pulse width which may have impacted the ability to recruit underlying Aβ fibers.

The ability of 600 Hz HFBS to recruit Aβ fibers at smaller amplitudes than LFTS may explain the ability of HFBS to allow the subject to sense a passive change in knee angle in a manner more closely resembling baseline capacity than LFTS. A previous study observed that axonal recruitment via SCS is primarily dependent upon stimulation amplitude and pulse width, with increases in either parameter leading to production of larger electric fields influencing more underlying neuronal structures.[3] It is possible that the unique combination of 600 Hz intraburst patterning with a 40 Hz interbust interval represents a stimulus within the functional and/or optimal ranges of both sensory pathways (i.e., pain and proprioception) to allow inhibition of the former and preservation of the latter.

Although a significant difference in EMG module complexity was not observed between stimulus modalities, the findings from proprioceptive testing during TTDPM may shed light on observed differences in raw EMG activity of certain muscles during the walking task. TA activity was seen to be active at inappropriate times during LFTS, which was not observed during HFBS. Specifically, TA activity during the late stance phase of the gait cycle was elevated compared to HFBS and no stimulation trials and may contribute to a lack of propulsion during gait. We speculate that the interference in

proprioceptive signaling observed during TTDPM may have led to TA activity being improperly regulated by sensory afferents normally responsible for inhibition of antagonistic flexor activity during extension. Similar dysregulation, although not observed, may also be responsible for the lack of foot height through gait seen during LFTS and may account for the similarity between baseline trials with no stimulation and trials during HFBS. These findings highlight increased interest in neuromodulation of sensorimotor pathways using lower thoracic SCS, where a current clinical trial (NCT03586882) is investigating the effect of SCS on gait and balance in subjects with chronic pain.

Possible limitations of the presented study also warrant discussion. The potential of SCS to influence sensorimotor pathways of the spinal cord after stimulation has ended is not well understood and not explored in this study. For instance, various forms of neuromodulation of the cerebrum lead to carryover effects lasting longer than the duration of modulation. It is plausible that neuromodulation of the spinal cord may share similar principles and presented data may not represent, exclusively, effects of a single parameter type. Furthermore, data collection during intraoperative investigation was limited to 20 minutes and limited the ability to explore a larger parameter space of the SCS system. Finally, as highlighted previously, our findings represent data from only one individual.

In conclusion, we found in one subject that HFBS simultaneously activates more muscle groups and spares more proprioceptive signals than LFTS, which is a classical form of stimulation used in past investigations of motor recovery after spinal cord injury. It is shown that HFBS has the ability to recruit lower MNs at 1) lower stimulation amplitude 2) without disrupting proprioceptive signaling and 3) without influencing physiologically and kinematically appropriate mechanisms involved with human gait.

5.0 REFERENCES

1. Thompson, S. (2016). Spinal cord stimulation: Its Role in Managing Chronic Disease Symptoms. *International Neuromodulation Society.* Retrieved from http://www.neuromodulation.com/spinal-cord-stimulation.

2. North, R. B., Ewend, M. G., Lawton, M. T., & Piantadosi, S. (1991). Spinal cord stimulation for chronic, intractable pain: Superiority of “multi-channel” devices. *Pain*,*44*(2), 119–130. https://doi.org/10.1016/0304-3959(91)90125-H

3. Formento, E., Minassian, K., Wagner, F., Baptiste Mignardot, J., Le Goff-Mignardot, C. G., Rowald, A., … Courtine, G. (2018). Electrical spinal cord stimulation must preserve proprioception to enable locomotion in humans with spinal cord injury. https://doi.org/10.1038/s41593-018-0262-6

4. Cheung, V. C. K. (2005). Central and Sensory Contributions to the Activation and Organization of Muscle Synergies during Natural Motor Behaviors. *Journal of Neuroscience*. https://doi.org/10.1523/jneurosci.4904-04.2005

5. Pierrot-Deseilligny, E., & Burke, D. (2012). The circuitry of the human spinal cord: Spinal and corticospinal mechanisms of movement. In *The Circuitry of the Human Spinal Cord: Spinal and Corticospinal Mechanisms of Movement*. https://doi.org/10.1017/CBO9781139026727

6. Harkema, S., Hodes, J., Angeli, C., Chen, Y., Ferreira, C., Willhite, A. B., … Grossman, R. G. (2011). Effect of epidural stimulation of the lumbosacral spinal cord on voluntary movement, standing, and assisted stepping after motor complete paraplegia: a case study. *The Lancet*, *377*, 1938–1947. https://doi.org/10.1016/S0140

7. van den Heuvel, L. L. (2014). Stahl’s essential psychopharmacology: Neuroscientific basis and practical applications (4th edition). In *Journal of Child & Adolescent Mental Health* (Vol. 26, Issue 2). https://doi.org/10.2989/17280583.2014.914944

8. Bear, M. F., Connors, B. W., & Paradiso, M. A. (2015). Neuroscience: Exploring the brain: Fourth edition. In *Neuroscience: Exploring the Brain: Fourth Edition*.

9. Luo, J., Feng, J., Liu, S., Walters, E. T., & Hu, H. (2015). Molecular and cellular mechanisms that initiate pain and itch. *Cellular and Molecular Life Sciences*, *72*(17), 3201–3223. https://doi.org/10.1007/s00018-015-1904-4

10. Huang, J., Polgár, E., Solinski, H. J., Mishra, S. K., Tseng, P. Y., Iwagaki, N., Boyle, K. A., Dickie, A. C., Kriegbaum, M. C., Wildner, H., Zeilhofer, H. U., Watanabe, M., Riddell, J. S., Todd, A. J., & Hoon, M. A. (2018). Circuit dissection of the role of somatostatin in itch and pain. *Nature Neuroscience*, *21*(5), 707–716. https://doi.org/10.1038/s41593-018-0119-z

11. Steeds, C. E. (2016). The anatomy and physiology of pain. In *Surgery (United Kingdom)* (Vol. 34, Issue 2, pp. 55–59). https://doi.org/10.1016/j.mpsur.2015.11.005

12. Nicholas, M., Vlaeyen, J. W. S., Rief, W., Barke, A., Aziz, Q., Benoliel, R., Cohen, M., Evers, S., Giamberardino, M. A., Goebel, A., Korwisi, B., Perrot, S., Svensson, P., Wang, S. J., & Treede, R. D. (2019). The IASP classification of chronic pain for ICD-11: Chronic primary pain. In *Pain* (Vol. 160, Issue 1, pp. 28–37). https://doi.org/10.1097/j.pain.0000000000001390

13. (IHME)., I. for H. M. and E. (2018). *Findings from the GBD*. www.healthdata.org

14. Scholz, J., Finnerup, N. B., Attal, N., Aziz, Q., Baron, R., Bennett, M. I., Benoliel, R., Cohen, M., Cruccu, G., Davis, K. D., Evers, S., First, M., Giamberardino, M. A., Hansson, P., Kaasa, S., Korwisi, B., Kosek, E., Lavand'Homme, P., Nicholas, M., … Treede, R. D. (2019). The IASP classification of chronic pain for ICD-11: Chronic neuropathic pain. In *Pain* (Vol. 160, Issue 1, pp. 53–59). https://doi.org/10.1097/j.pain.0000000000001365

15. De Biasi, S., & Rustioni, A. (1988). Glutamate and substance P coexist in primary afferent terminals in the superficial laminae of spinal cord. In *Proceedings of the National Academy of Sciences of the United States of America* (Vol. 85, Issue 20). https://doi.org/10.1073/pnas.85.20.7820

16. Nakamura-Craig, M., & Gill, B. K. (1991). Effect of neurokinin A, substance P and calcitonin gene related peptide in peripheral hyperalgesia in the rat paw. *Neuroscience Letters*, *124*(1), 49–51. https://doi.org/10.1016/0304-3940(91)90819-F

17. Hagermark, O., Hokfelt, T., & Pernow, B. (1978). Flare and itch induced by substance P in human skin. *Journal of Investigative Dermatology*. https://doi.org/10.1111/1523-1747.ep12515092

18. Peng, J., Gu, N., Zhou, L., B Eyo, U., Murugan, M., Gan, W. B., & Wu, L. J. (2016). Microglia and monocytes synergistically promote the transition from acute to chronic pain after nerve injury. *Nature Communications*, *7*. https://doi.org/10.1038/ncomms12029

19. Melzack, R., & Wall, P. D. (1965). Pain Mechanisms: A New Theory. *Science*, *150*(3699), 971 LP – 979. https://doi.org/10.1126/science.150.3699.971

20. Shealy, C. N., Mortimer, J. T., & Reswick, J. B. (1967). Electrical inhibition of pain by stimulation of the dorsal columns: preliminary clinical report. *Anesthesia and Analgesia*, *46*(4), 489–491. https://doi.org/10.1213/00000539-196707000-00025

21. Deer T.R. (2016) Programming Spinal Cord Stimulation Systems. In: Deer T., Pope J. (eds) Atlas of Implantable Therapies for Pain Management. Springer, New York, NY

22. Spectra WaveWriter™ SCS System. (n.d.). Retrieved March 24, 2020, from https://www.bostonscientific.com/en-US/products/spinal-cord-stimulator-systems/spectra-wavewriter-scs.html

23. Kapural, L., Yu, C., Doust, M. W., Gliner, B. E., Vallejo, R., Todd Sitzman, B., Amirdelfan, K., Morgan, D. M., Brown, L. L., Yearwood, T. L., Bundschu, R., Burton, A. W., Yang, T., Benyamin, R., & Burgher, A. H. (2015). Novel 10-kHz High-frequency Therapy (HF10 Therapy) Is Superior to Traditional Low-frequency Spinal Cord Stimulation for the Treatment of Chronic Back and Leg Pain. *Anesthesiology*, *123*(4), 851–860. https://doi.org/10.1097/ALN.0000000000000774

24. Deer, T., Slavin, K. V., Amirdelfan, K., North, R. B., Burton, A. W., Yearwood, T. L., Tavel, E., Staats, P., Falowski, S., Pope, J., Justiz, R., Fabi, A. Y., Taghva, A., Paicius, R., Houden, T., & Wilson, D. (2018). Success Using Neuromodulation With BURST (SUNBURST) Study: Results From a Prospective, Randomized Controlled Trial Using a Novel Burst Waveform. *Neuromodulation*, *21*(1), 56–66. https://doi.org/10.1111/ner.12698

25. Ertekin, C., Mungan, B., & Uludağ, B. (1996). Sacral cord conduction time of the soleus H-reflex. *Journal of Clinical Neurophysiology*, *13*(1), 77–83. https://doi.org/10.1097/00004691-199601000-00008

26. Lloyd, D. P. C. (1946). Integrative pattern of excitation and inhibition in two-neuron reflex arcs. *Journal of Neurophysiology*, *9*(6), 439–444. https://doi.org/10.1152/jn.1946.9.6.439

27. Crone, C., Hultborn, H., Jespersen, B., & Nielsen, J. (1987). Reciprocal Ia inhibition between ankle flexors and extensors in man. *The Journal of Physiology*, *389*(1), 163–185. https://doi.org/10.1113/jphysiol.1987.sp016652

28. Dietz, V., & Colombo, G. (1998). Influence of body load on the gait pattern in Parkinson's disease. *Movement Disorders*, *13*(2), 255–261. https://doi.org/10.1002/mds.870130210

29. Andersen, O. K., Sonnenborg, F. A., & Arendt-Nielsen, L. (1999). Modular organization of human leg withdrawal reflexes elicited by electrical stimulation of the foot sole. *Muscle and Nerve*, *22*(11), 1520–1530. https://doi.org/10.1002/(SICI)1097-4598(199911)22:11<1520::AID-MUS6>3.0.CO;2-V

30. Spaich, E. G., Arendt-Nielsen, L., & Andersen, O. K. (2004). Modulation of Lower Limb Withdrawal Reflexes during Gait: A Topographical Study. *Journal of Neurophysiology*, *91*(1), 258–266. https://doi.org/10.1152/jn.00360.2003

31. Clark, D. J., Ting, L. H., Zajac, F. E., Neptune, R. R., & Kautz, S. A. (2010). Merging of healthy motor modules predicts reduced locomotor performance and muscle coordination complexity post-stroke. *Journal of Neurophysiology*, *103*(2), 844–857. https://doi.org/10.1152/jn.00825.2009

32. Ivanenko, Y. P., Poppele, R. E., & Lacquaniti, F. (2004). Five basic muscle activation patterns account for muscle activity during human locomotion. *Journal of Physiology*, *556*(1), 267–282. https://doi.org/10.1113/jphysiol.2003.057174

33. Wagner, F. B., Mignardot, J. B., Le Goff-Mignardot, C. G., Demesmaeker, R., Komi, S., Capogrosso, M., Rowald, A., Seáñez, I., Caban, M., Pirondini, E., Vat, M., McCracken, L. A., Heimgartner, R., Fodor, I., Watrin, A., Seguin, P., Paoles, E., Van Den Keybus, K., Eberle, G., … Courtine, G. (2018). Targeted neurotechnology restores walking in humans with spinal cord injury. *Nature*, *563*(7729), 65–93. https://doi.org/10.1038/s41586-018-0649-2

34. Leeman, S. A. (2007). SSEPs: From limb to cortex. In *Neurodiagnostic Journal* (Vol. 47, Issue 3, pp. 165–177). https://doi.org/10.1080/1086508x.2007.11079628

35. Kumar, S. (2017). Electromyography in ergonomics. In *Electromyography in Ergonomics*. https://doi.org/10.1201/9780203758670

36. Boroojerdi, B., Battaglia, F., Muellbacher, W., & Cohen, L. G. (2001). Mechanisms influencing stimulus-response properties of the human corticospinal system. In *Clinical Neurophysiology* (Vol. 112, Issue 5). https://doi.org/10.1016/S1388-2457(01)00523-5

37. Nagai, T., Sell, T. C., House, A. J., Abt, J. P., & Lephart, S. M. (2013). Knee proprioception and strength and landing kinematics during a single-leg stop-jump task. *Journal of Athletic Training*, *48*(1), 31–38. https://doi.org/10.4085/1062-6050-48.1.14

38. Bowden, M. G., Clark, D. J., & Kautz, S. A. (2010). Evaluation of abnormal synergy patterns poststroke: Relationship of the fugl-meyer assessment to hemiparetic locomotion. *Neurorehabilitation and Neural Repair*

39. Garza-Ulloa, J. (2018). Application of mathematical models in biomechatronics: artificial intelligence and time-frequency analysis. In *Applied Biomechatronics using Mathematical Models* (pp. 373–524). https://doi.org/10.1016/b978-0-12-812594-6.00006-8

40. Cheung, A. S., Gray, H., Schache, A. G., Hoermann, R., Lim Joon, D., Zajac, J. D., Pandy, M. G., & Grossmann, M. (2017). Androgen deprivation causes selective deficits in the biomechanical leg muscle function of men during walking: a prospective case–control study. *Journal of Cachexia, Sarcopenia and Muscle*, *8*(1), 102–112. https://doi.org/10.1002/jcsm.12133